applied sciences

MDPI

Article

Controlling Composite TiO_2 Powder Characteristics in the Solid-State Synthesis of $BaTiO_3$ Powders for Improved Sintering and Permittivity: A Comparative Study

Sang-Heun Lee [1,2,†], Yoon-Seok Lee [1,†], Jandi Kim [1,2], Ji-Hye Seo [1,2], Myunghee Cho [1,3], Hun Kwak [1], Ran-Sae Cheon [1,2], Seungchan Cho [4], Yangdo Kim [2,*], Kyoung-Seok Moon [3] and Moonhee Choi [1,*]

1 Electronic Convergence Division, Korea Institute of Ceramic Engineering and Technology, 101 Soho-Ro, Jinju 52851, Republic of Korea; hkwak@kicet.re.kr (H.K.)
2 School of Materials Science and Engineering, Pusan National University, Busan 46241, Republic of Korea
3 Department of Materials Engineering and Convergence Technology, School of Materials Science and Engineering, Gyeongsang National University, Jinju 52828, Republic of Korea; ksky.moon@gnu.ac.kr
4 Composites Research Division, Korea Institute of Materials Science, Changwon 51508, Republic of Korea; sccho@kims.re.kr
* Correspondence: yangdo@pusan.ac.kr (Y.K.); moonhee77.choi@kicet.re.kr (M.C.)
† These authors contributed equally to this work.

Abstract: In this study, the anatase–rutile phase fraction of TiO_2, which would play a vital role in the solid-state synthesis of $BaTiO_3$, was controlled to form a composite phase. The composite TiO_2 was applied to a solid-state synthesis reaction, and the tetragonality, dielectric properties, and microstructure of the resulting $BaTiO_3$ powders were analyzed under different synthesis conditions of TiO_2. Furthermore, a comparative analysis of solid-state-synthesized $BaTiO_3$ powders prepared using anatase, rutile, and mixed (anatase + rutile) TiO_2 was performed to elucidate the mechanism of improvement in the sintering behavior and dielectric properties of the $BaTiO_3$ powder synthesized using the composite TiO_2. As a result of applying composite TiO_2, $BaTiO_3$ powder with excellent tetragonality was synthesized. In addition, it is effective in powder growth and the control of powder morphology, so sintering and dielectric properties can be improved at relatively low temperatures.

Keywords: $BaTiO_3$; TiO_2; dielectric; solid-state synthesis; multilayer ceramic capacitors

check for updates

Citation: Lee, S.-H.; Lee, Y.-S.; Kim, J.; Seo, J.-H.; Cho, M.; Kwak, H.; Cheon, R.-S.; Cho, S.; Kim, Y.; Moon, K.-S.; et al. Controlling Composite TiO_2 Powder Characteristics in the Solid-State Synthesis of $BaTiO_3$ Powders for Improved Sintering and Permittivity: A Comparative Study. *Appl. Sci.* **2023**, *13*, 9720. https://doi.org/10.3390/app13179720

Academic Editor: Domingo Pérez-Coll

Received: 3 August 2023
Revised: 17 August 2023
Accepted: 24 August 2023
Published: 28 August 2023

Copyright: © 2023 by the authors. Licensee MDPI, Basel, Switzerland. This article is an open access article distributed under the terms and conditions of the Creative Commons Attribution (CC BY) license (https://creativecommons.org/licenses/by/4.0/).

1. Introduction

Recently, research and development (R&D) related to future mobility solutions, including electric vehicles (EVs), have received increasing attention to foster clean, sustainable mobility and the development of electronic equipment components for next-generation communication technologies, such as 5G and 6G. As a result, the demand for passive components in electronic devices with a high energy density and high power density has increased. In particular, active R&D has been focused on the miniaturization of multilayer ceramic capacitors (MLCCs), which account for the largest proportion of passive components [1,2]. The miniaturization of electronic products leads to the issue of limited mounting space for the electronic components. To address this limitation, the development of ultra-thin MLCCs is essential. $BaTiO_3$, a typical ferroelectric, has a high dielectric constant at room temperature, low dielectric loss, and excellent insulation resistance, so it is used as a main raw material for MLCC. Generally, perovskite-structured small-sized ferroelectric $BaTiO_3$ powders are first synthesized, and then, dielectric slurries are prepared for fabricating a few micrometer-thick dielectric sheets. These sheets are then stacked to form hundreds of layers to produce a compact, high-capacitance MLCC [3,4]. Typically, $BaTiO_3$ powders for application in miniature MLCCs are prepared via hydrothermal synthesis. The hydrothermal synthesis method is advantageous for the preparation of homogeneous $BaTiO_3$ particles with a narrow size distribution [5–9]. In particular, nanopowder synthesis

using this method is simple, as the process does not involve any heat treatments. However, in the case of the $BaTiO_3$ powder synthesized through the hydrothermal method, the lattice hydroxyl groups (–OH) attack the oxygen lattice, forming oxygen vacancies through a charge compensation mechanism. The hydroxyl defects develop into intragranular pores, which results in a decrease in the dielectric constant [10,11]. Furthermore, during $BaTiO_3$ grain growth via Ostwald ripening at temperatures of 800 °C or higher, internal pores coalesce and grow. Consequently, defects are inevitably present in $BaTiO_3$ synthesized through the hydrothermal method [12]. Recently, significant efforts have been devoted to the R&D of MLCCs for diverse applications, such as electric/electronic parts for the automotive industry. This has led to a growing interest in the R&D of the solid-state synthesis of $BaTiO_3$ rather than the hydrothermal synthesis of $BaTiO_3$, as the former is conducive to particle size atomization [13,14]. In the solid-state synthesis of $BaTiO_3$, powders of carbonates and oxides, such as $BaCO_3$ and TiO_2, are mixed, and solid-state reaction with heat treatment at appropriate high temperatures is subsequently performed. During this process, Ba^{2+} ions diffuse into the TiO_2 surface and form an initial $BaTiO_3$ layer at the $BaCO_3/TiO_2$ grain boundaries. Continuous reaction of the as-formed layer with $BaCO_3$ results in the formation of a Ba_2TiO_4 intermediate phase. Subsequently, with a continuous supply of thermal energy through heat treatment, $BaTiO_3$ is produced through the reaction between Ba_2TiO_4 and TiO_2. The diffusion of Ba^{2+} ions at the TiO_2 interface is the key mechanism of the solid-state synthesis reaction [1,13,15–21].

In this study, TiO_2, an important component in the solid-state synthesis reaction of $BaTiO_3$, was controlled, and the corresponding changes in various properties of solid-state-synthesized $BaTiO_3$ powders were examined. Anatase- and rutile-phase TiO_2 have different diffusion rates and reaction rates due to their different crystal structures. Therefore, $BaTiO_3$ powder was prepared by controlling the ratio of the two phases with different properties of TiO_2, and the change in properties was examined. The composite TiO_2 was synthesized by heat-treating anatase TiO_2 to control the anatase–rutile phase ratio. In order to assess the effect of composite TiO_2 on the solid-state synthesis of $BaTiO_3$, mixed TiO_2 with the same phase ratio and a reference TiO_2 (anatase, rutile) were also prepared. The prepared TiO_2 was applied to the solid-phase synthesis of $BaTiO_3$, and the effect of the composite TiO_2 with a controlled anatase–rutile phase ratio on the properties of $BaTiO_3$ was investigated in detail.

2. Experimental Section

2.1. Preparation of Composite TiO_2

For the preparation of composite TiO_2, 80 nm anatase TiO_2 (purity > 99.8%, Ditto Technology Co., Ltd., Gunpo, Republic of Korea) was used as the starting material. To control the anatase–rutile phase ratio, heat treatment was performed at a temperature range of 800 to 900 °C for 1 to 9 h. In addition, anatase TiO_2 and 60 nm rutile TiO_2 (purity > 99.8%, Armstec Ind. Co., Ltd., Hwaseong, Republic of Korea) were weighed and mixed such that the anatase–rutile phase ratio matched with that of the heated composite TiO_2.

2.2. Solid-State Synthesis of $BaTiO_3$

For the solid-state synthesis of $BaTiO_3$, 150 nm $BaCO_3$ (purity > 99.8%, Qingdao Terio Corporation, Qingdao, China) and TiO_2 (anatase, rutile, composite, and mixed TiO_2) were mixed at a ratio of 1:1 in moles. To ensure uniform dispersion, a dispersing agent (DISPERBYK-111, BYK Additives & Instruments, Wesel, Germany) and ethanol (ethyl alcohol 99.5%, Daejung Chemicals & Metals Co., Ltd., Siheung, Republic of Korea) were added, and ball milling was performed for 24 h using 3 Φ beads. After ball milling, the powder was dried in an exhaust-fan-type oven at 100 °C for 24 h to remove ethanol. For the synthesis of $BaTiO_3$ powder using the dried mixed powder, calcination was performed for 2 h at a heating rate of 5 °C/min at temperatures of 1000 to 1100 °C in an air atmosphere.

2.3. Fabrication of Sintered Specimens

To the calcinated powder, 10 wt% polyvinyl alcohol (PVA 1500, Daejung Chemicals & Metals Co., Ltd., Siheung, Republic of Korea) was added, and the mixture was compressed at a pressure of 127 MPa for 1 min. Twenty round disk-shaped specimens of 10 Φ size were fabricated under uniaxial compression for each condition. After loading the fabricated disk specimens into a furnace, the specimens were sintered at 1300 °C for 2 h in an air atmosphere at a heating rate of 5 °C/min. Ag paste was applied to the sintered disk specimens, which were heated at 700 °C for 10 min at a heating rate of 1 °C/min to form an external electrode.

2.4. Evaluation

2.4.1. Dielectric Properties

Dielectric properties were evaluated under the conditions of 1 kHz and 1 V at ambient temperature using an LCR meter (E4980A, KEYSIGHT TECHNOLOGIES, Santa Rosa, CA, USA). In addition, the change in the value of the dielectric constant was observed by varying the temperature (from −55 to 160 °C).

2.4.2. Determination of the Crystal Structure

The crystal structures of composite TiO_2 prepared through heat treatment and the synthesized powder were determined via X-ray diffraction (XRD) using Cu Kα radiation (λ = 1.54 Å) in the 2θ range of 20° to 80° (D8 Advance A25, BRUKER, Billerica, MA, USA). The following equation was used, considering the intensity of the main XRD peak (101/110), to obtain the ratio of the anatase and rutile phases of the composite TiO_2 under each heat treatment condition [22]:

$$R(T) = 0.679\frac{I_R}{I_R + I_A} + 0.312\left(\frac{I_R}{I_R + I_A}\right)^2$$

where *R(T)* indicates the content (%) of the rutile phase at temperature *T*, whereas I_A and I_R denote the intensity of the main peak of the anatase (main peak = (101), 2Θ = 25.3°) and rutile phases (main peak = (110), 2Θ = 27.44°), respectively. In XRD analysis, Rietveld refinement was used to determine the tetragonality (c/a) of the $BaTiO_3$ powder.

2.4.3. Microstructure

The microstructure and crystal structure of the composite TiO_2 powder prepared through heat treatment were characterized using high-resolution transmission electron microscopy (HRTEM, JEM-4010, JEOL Ltd., Tokyo, Japan). The morphology and size of particles and grains in the microstructure of the as-synthesized $BaTiO_3$ powder and sintered specimens were analyzed using field-emission scanning electron microscopy (FE-SEM, CLARA, TESCAN, Brno, Czech Republic).

3. Results and Discussion

Anatase TiO_2 with a particle size of 80 nm was pre-annealed at a temperature range of 800 to 900 °C for 1 to 12 h. Characterization of the anatase TiO_2 powder pre-annealed at 800 °C for 1 h revealed the typical crystal structure of anatase TiO_2. When the pre-annealing time was varied in the range of 3 to 5 h, the fraction of the rutile phase increased, as confirmed via XRD analysis. After pre-annealing at a temperature of 800 °C for 5 h, anatase–rutile composite TiO_2 powder with 18% rutile TiO_2 was obtained. When the temperature was increased to 850 °C and the annealing time was increased, a smooth transformation of the anatase to the rutile phase was achieved. After annealing at 900 °C, an analysis of the resulting crystal structure showed that most of the TiO_2 underwent phase transformation to form rutile TiO_2 within a short annealing time (Figure 1a,b). Therefore, the crystal structure analysis results reveal that controlling the anatase–rutile phase fraction of the composite TiO_2 to form different crystal structures is possible by altering the pre-annealing conditions

(Figure 1c). In the subsequent solid-state synthesis of $BaTiO_3$, TiO_2 samples obtained under pre-annealing conditions #1 to #3 and #5 were used (Figure 1d).

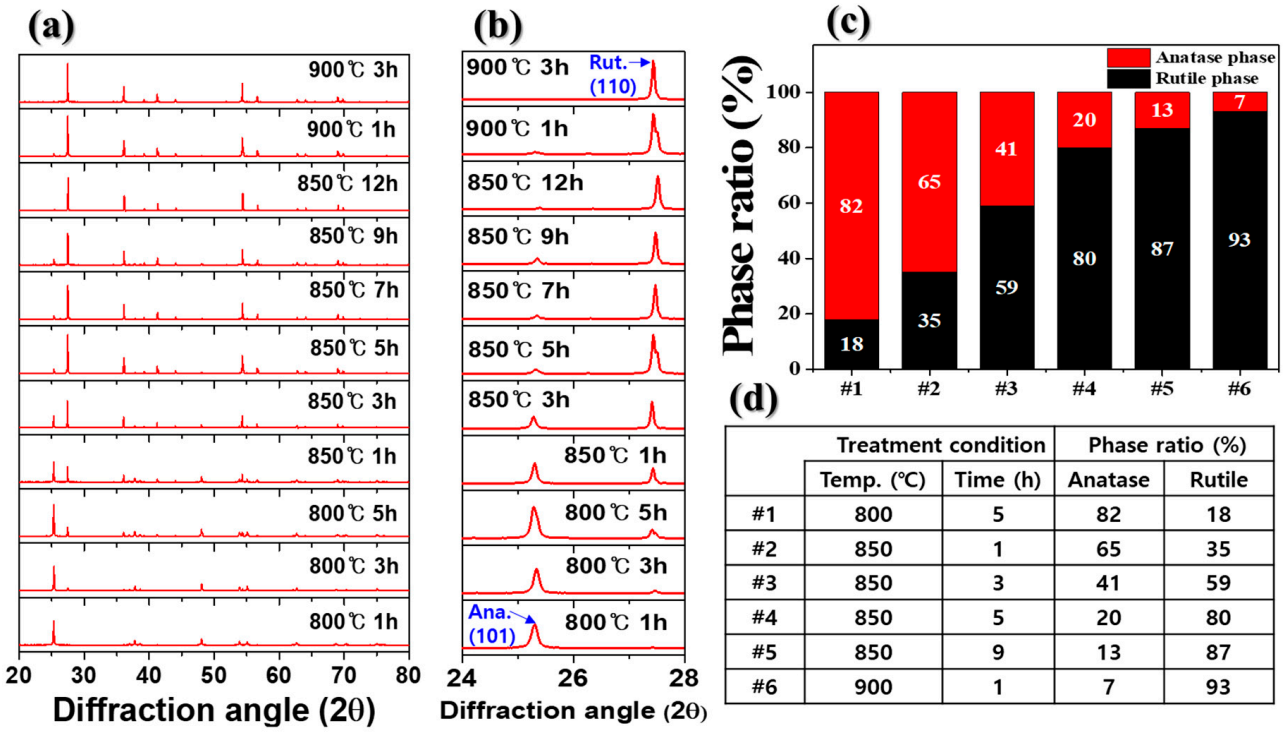

(d)

	Treatment condition		Phase ratio (%)	
	Temp. (℃)	Time (h)	Anatase	Rutile
#1	800	5	82	18
#2	850	1	65	35
#3	850	3	41	59
#4	850	5	20	80
#5	850	9	13	87
#6	900	1	7	93

Figure 1. Analysis of changes in the crystal structure and composite phase ratio according to the heat treatment conditions: (**a**) Anatase TiO_2. (**b**) XRD characterization. (**c**) Anatase–rutile phase ratio under different treatment conditions. (**d**) TiO_2 treatment conditions for the experiment on the solid-state synthesis of $BaTiO_3$.

The anatase phase of TiO_2 has an unstable crystal structure, and under specific temperature conditions, it spontaneously transforms into rutile TiO_2, which is a stable phase [23–27]. The crystal structure analysis showed that the phase transformation of the anatase TiO_2 to the crystal structure exhibiting a composite phase with approximately 18% rutile phase occurred under the conditions of annealing at 800 °C for 5 h (Figure 1). Figure 2 shows the results of the HRTEM analysis of the annealed TiO_2 powder. Grains of larger and smaller sizes were observed in the powder. Fast Fourier transformation (FFT) analysis of the HRTEM images confirmed that the larger grains possessed the anatase crystal structure, whereas smaller grains were rutile phase TiO_2. These observations indicate that when anatase TiO_2 was annealed at the given temperature, small grains could transform to the rutile phase.

Mixed powders were prepared by mixing TiO_2 synthesized under different annealing conditions (#1 to #3; #5) with $BaCO_3$ with a molar ratio of 1:1. In addition, anatase and rutile TiO_2 powders were mixed to ensure that the anatase–rutile phase ratio was the same as that of the heated TiO_2 powder prepared under respective annealing conditions. The prepared TiO_2 powder was mixed with $BaCO_3$ at a molar ratio of 1:1 to obtain a $BaCO_3$–TiO_2 powder. Furthermore, powders were prepared by separately mixing 100% anatase TiO_2 and 100% rutile TiO_2 with $BaCO_3$ at a molar ratio of 1:1 (Table 1).

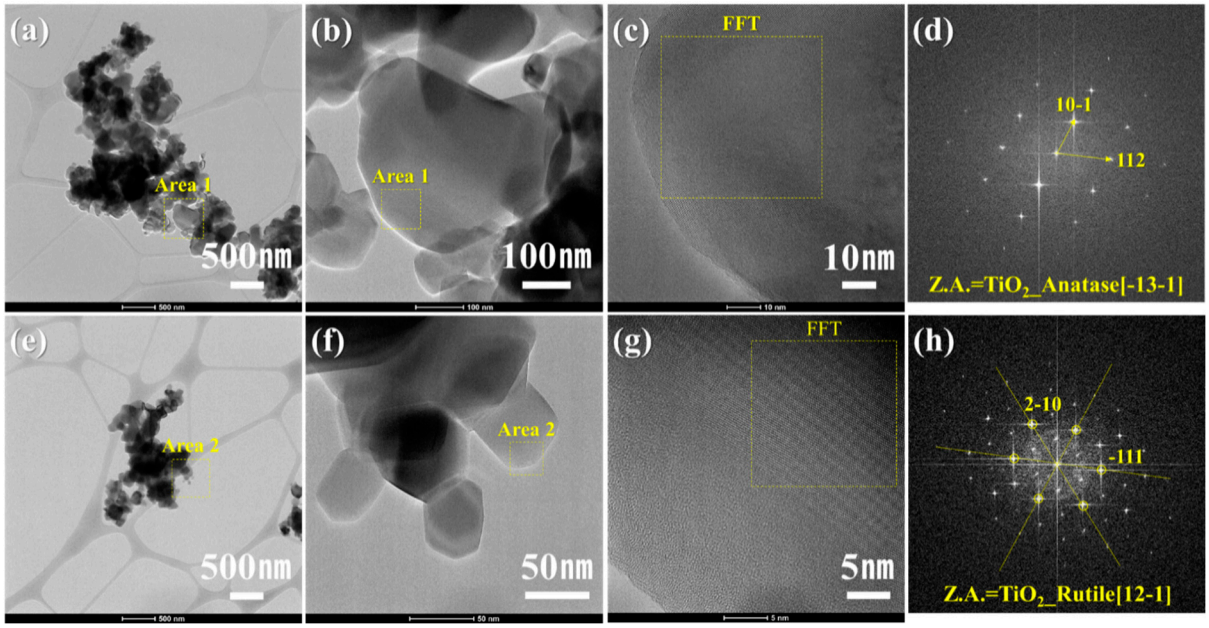

Figure 2. HRTEM and FFT analysis of TiO_2 powder annealed at 850 °C for 3 h: (**a**–**c**) HRTEM analysis results, (**d**) FFT analysis result of TiO_2 powder annealed at 850 °C for 3 h (Area 1), (**e**–**g**) HRTEM analysis results, and (**h**) FFT analysis result of TiO_2 powder annealed at 850 °C for 3 h (Area 2).

Table 1. Composition of prepared powders for the solid-state synthesis of $BaTiO_3$.

		TiO_2
Heated TiO_2	**BT#1**	#1
	BT#2	#2
	BT#3	#3
	BT#4	#5
Mixed TiO_2	**BT#5**	A:R = 82:18
	BT#6	A:R = 65:35
	BT#7	A:R = 41:59
	BT#8	A:R = 13:87
Ref.	**BT(A)**	Anatase TiO_2
	BT(R)	Rutile TiO_2

The $BaCO_3$–TiO_2 powders, mixed as described above, were calcined at 1000 and 1100 °C for 2 h. XRD analysis of the powders obtained via solid-state synthesis at 1000 °C under respective mixing conditions revealed the presence of typical $BaTiO_3$ crystal structures. By analyzing the diffractions from the (002) and (200) planes of the synthesized $BaTiO_3$ powders, a structure closely resembling a cubic structure, without distinct peak splitting of the (002) and (200) planes, was confirmed for the $BaTiO_3$ powder obtained via solid-state synthesis using 100% anatase TiO_2 and 100% rutile TiO_2, respectively (Figure 3a,b). In addition, observing clear 002/200 peak splitting was difficult in the case of the $BaTiO_3$ powder synthesized using a simple mixture of anatase and rutile TiO_2 powders. However, in the XRD patterns of the BT#1 to BT#4 powders synthesized using the composite TiO_2 powder prepared under the annealing conditions of #1 to #4, apparent 002/200 peak splitting appeared. In the case of $BaTiO_3$ powders BT#1 to BT#4 synthesized at a temperature of 1100 °C, apparent peak splitting was observed on the 002/200 planes.

However, 002/200 peak splitting was not apparent in the case of the BT#5 to BT#8 powders, which used the simply mixed TiO_2 powder.

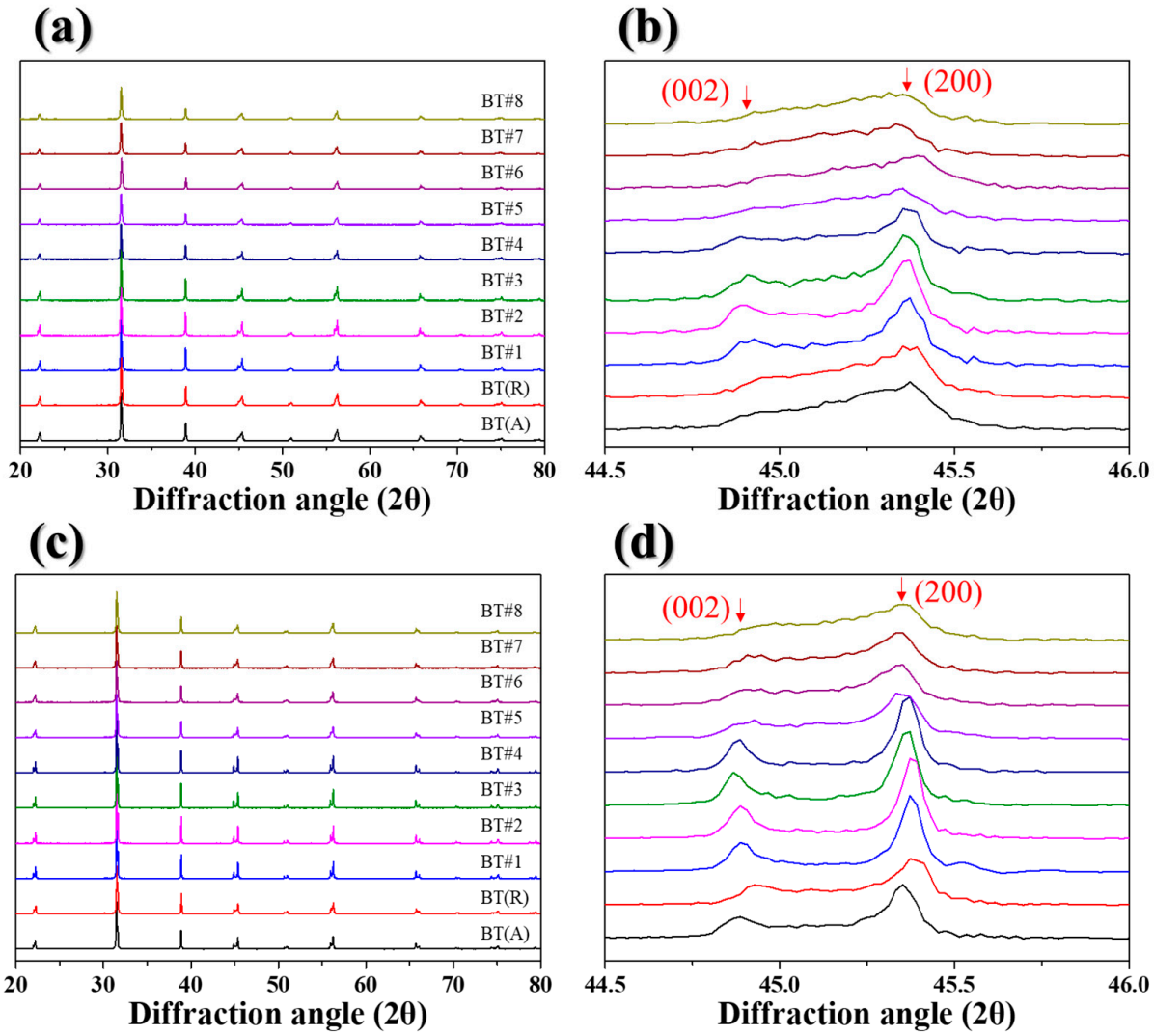

Figure 3. Characterization of crystal structures of $BaTiO_3$ powders prepared via solid-state synthesis under different TiO_2 conditions at two different temperatures: (**a**,**b**) 1000 °C × 2 h and (**c**,**d**) 1100 °C × 2 h.

Tetragonality (c/a ratio) means the ratio of the a-axis lattice constant to the c-axis lattice constant. Tetragonality is the source of the high dielectric properties of $BaTiO_3$ and is one of the important criteria used to evaluate ferroelectric $BaTiO_3$ powder. The a-axis and c-axis lattice constants were obtained by calculating the (200) and (002) peaks between 44 and 46° (2θ) of the measured XRD pattern using Rietveld analysis [28,29]. Rietveld refinement of the XRD results revealed that the $BaTiO_3$ powders synthesized using composite TiO_2 powders at 1000 and 1100 °C had excellent tetragonality values of 1.0094–1.01 (1000 °C) and 1.0102–1.0104 (1100 °C), respectively (Figure 4). However, when mixed TiO_2 was used for the synthesis, the resulting powders exhibited low tetragonality values of 1.0048–1.0076 (1000 °C) and 1.0077–1.0087 (1100 °C).

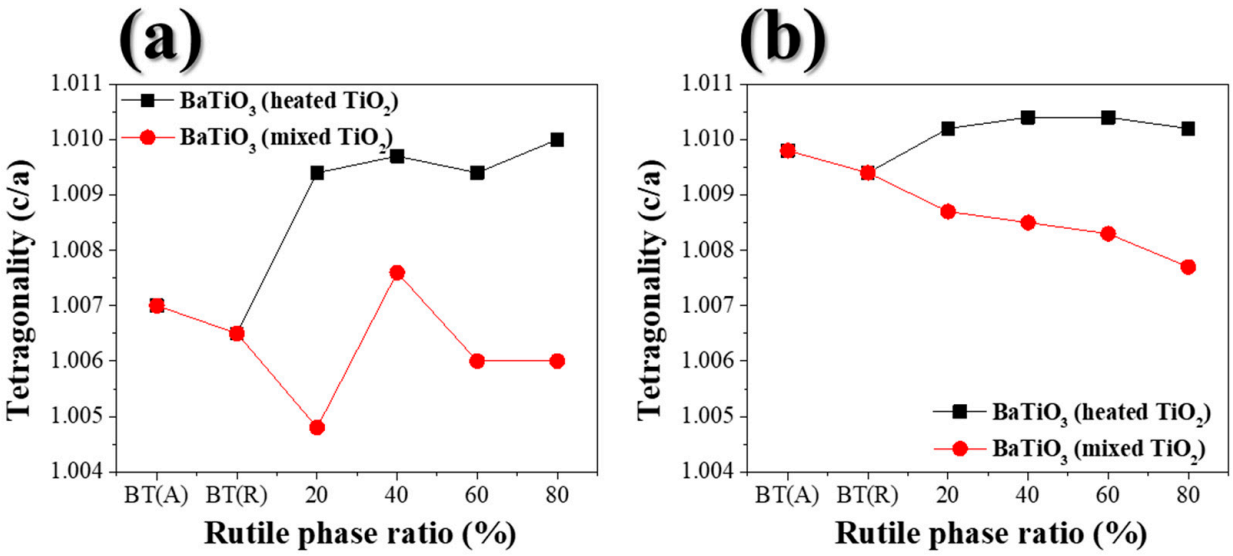

Figure 4. Tetragonality of $BaTiO_3$ prepared using different TiO_2 samples through solid-state synthesis via Rietveld analysis: (**a**) 1000 °C × 2 h and (**b**) 1100 °C × 2 h.

First, a solid-state synthesis reaction was performed at 1000 °C under the mixing conditions of BT(A) and BT(R). Microstructure observations conducted after the synthesis under the respective conditions revealed grain growth of the $BaTiO_3$ powders (Figure 5). The low tetragonality, as indicated by the XRD analysis results, is attributed to the lack of sufficient grain growth [30,31]. Furthermore, grain growth of the $BaTiO_3$ powders was confirmed when the solid-state synthesis was performed at 1000 °C under the mixing conditions of BT#1 to BT#4. However, under the mixing condition of BT#4, with the highest ratio of the rutile phase, atomized powders were observed to be agglomerated. In the case of powders synthesized under the mixing conditions of BT#5 to BT#8 at 1000 °C, grain growth was suppressed, compared to that of the powders synthesized using composite TiO_2.

Next, a solid-state synthesis reaction was performed at 1100 °C under the mixing conditions of BT(A) and BT(R). Observation of the resulting microstructure shows that grain growth progressed to a higher extent compared to that of the powders synthesized at 1000 °C (Figure 6). In the case of BT(A), the synthesized powders comprised spherical-shaped particles. However, in the case of BT(R), morphology analysis of the synthesized powder revealed high anisotropy at the edges and in the uniaxial direction. In the case of $BaTiO_3$ powders synthesized at 1100 °C under the mixing conditions of BT#1 to BT#4, the growth of grains with sizes in the range of 268–446 nm was observed. However, numerous grains suppressed for growth were observed, as in the case of the powder synthesized using BT#4 at 1000 °C. In the case of $BaTiO_3$ powders synthesized at 1100 °C under the mixing conditions of BT#5 to BT#8, no grain growth was observed. Furthermore, the powder morphology of edges and anisotropic shapes were similar to those observed for the powders synthesized under different synthesis conditions at 1000 °C. The microstructure analysis of $BaTiO_3$ powders synthesized via the solid-state method at each calcination temperature under the respective TiO_2 conditions demonstrated that isotropic $BaTiO_3$ powders were formed when annealed TiO_2 powders were used. In addition, grain growth of the powders could be easily achieved using annealed TiO_2.

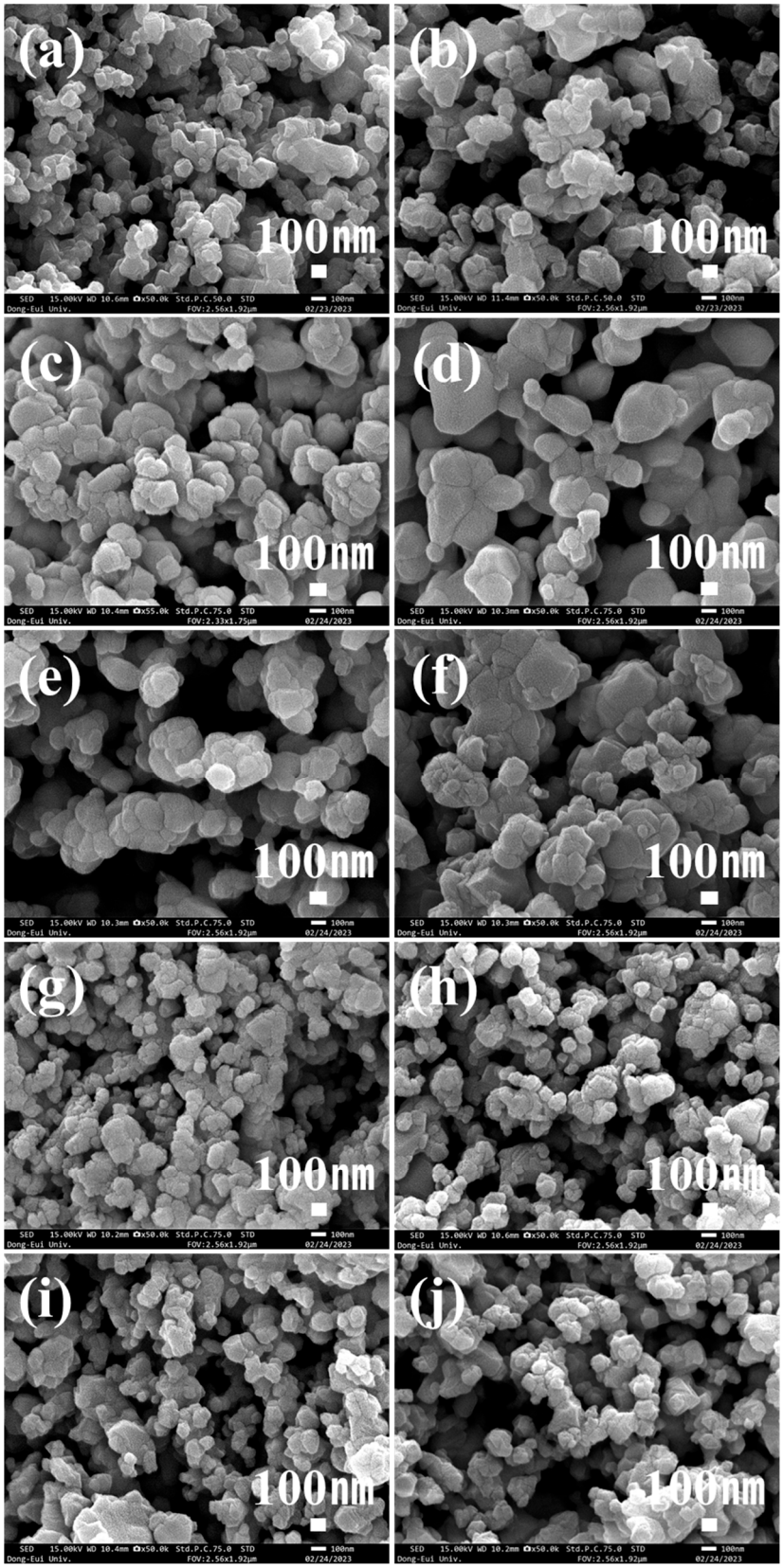

Figure 5. Microstructure of $BaTiO_3$ powders synthesized at 1000 °C under different TiO_2 conditions: (**a**) BT(A), (**b**) BT(R), (**c**) BT#1, (**d**) BT#2, (**e**) BT#3, (**f**) BT#4, (**g**) BT#5, (**h**) BT#6, (**i**) BT#7, and (**j**) BT#8.

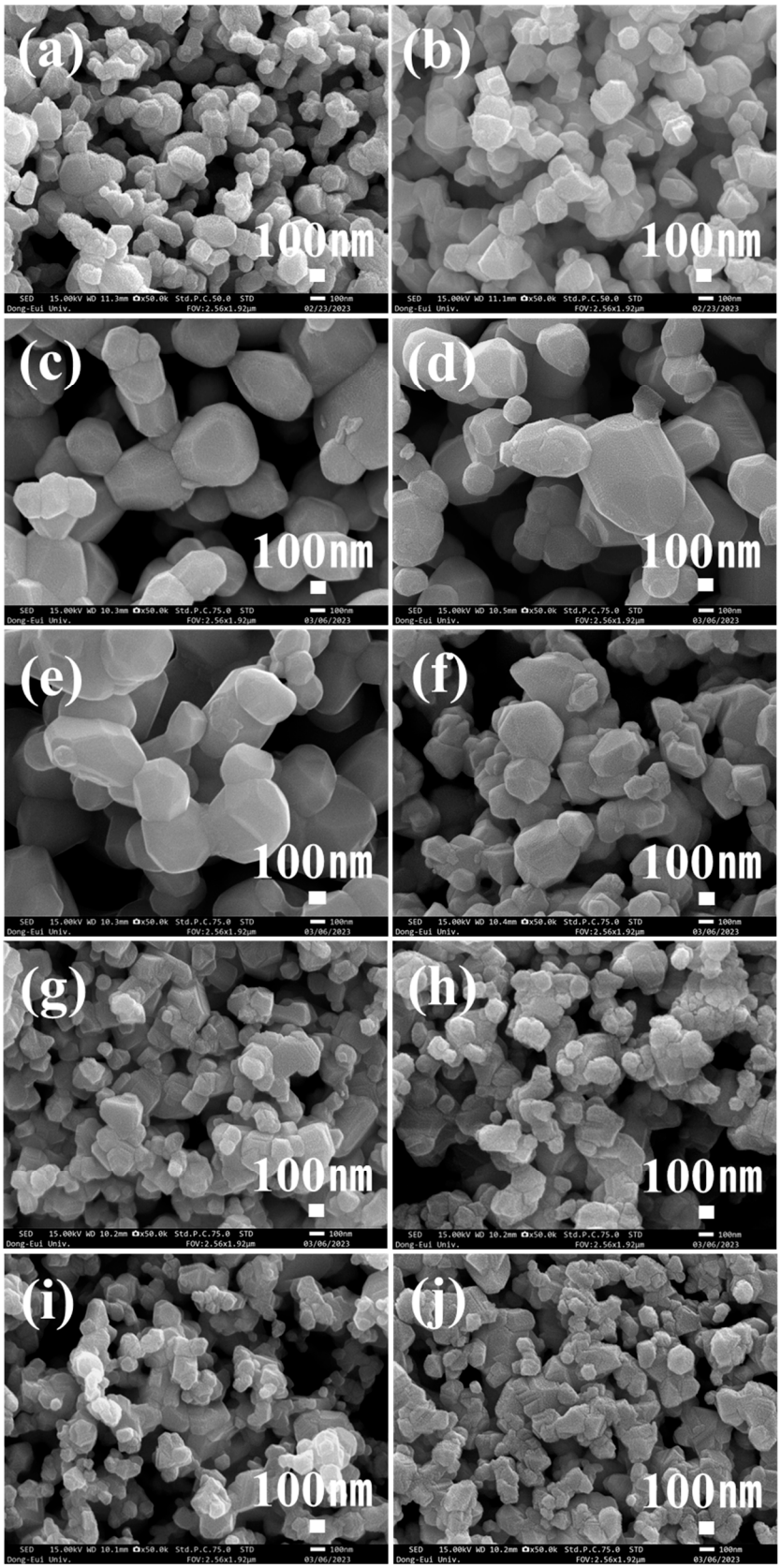

Figure 6. Microstructure of the $BaTiO_3$ powders synthesized at 1100 °C under different TiO_2 conditions: (**a**) BT(A), (**b**) BT(R), (**c**) BT#1, (**d**) BT#2, (**e**) BT#3, (**f**) BT#4, (**g**) BT#5, (**h**) BT#6, (**i**) BT#7, and (**j**) BT#8.

The calcination of $BaCO_3$ and TiO_2 resulted in the formation of $BaTiO_3$ through a solid-state synthesis reaction involving interfacial contact and diffusion between the materials (Figure 7). The solid-state synthesis reaction can be represented using the following equations.

$$BaCO_3 + TiO_2 \rightarrow BaTiO_3 + CO_2 \quad (1)$$

$$BaTiO_3 + BaCO_3 \rightarrow Ba_2TiO_4 + CO_2 \quad (2)$$

$$Ba_2TiO_4 + TiO_2 \rightarrow 2BaTiO_3 \quad (3)$$

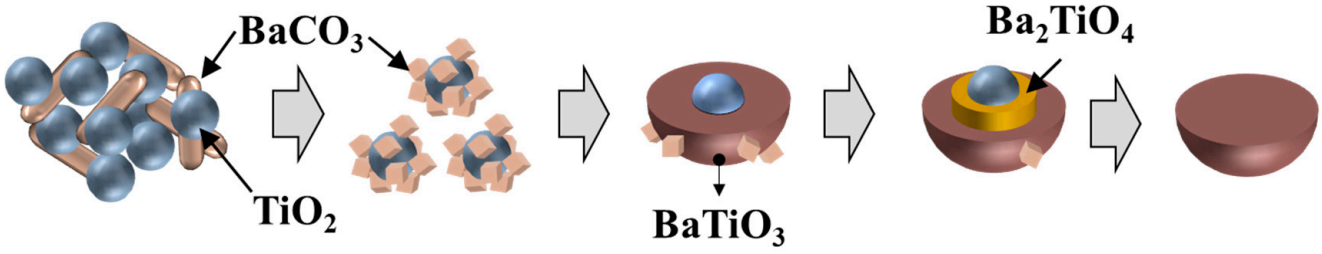

Figure 7. Schematic of solid-state synthesis using $BaCO_3$ and TiO_2.

At the initial stage of the reaction, $BaCO_3$ contacts the surface of TiO_2, and $BaTiO_3$ is formed via diffusion and an interface reaction (Equation (1)). The continuous adsorption of $BaCO_3$ and diffusion of ions result in the development of an intermediate-phase Ba_2TiO_4 (Equation (2)). Finally, Ba^{2+} ions diffuse to the inside of TiO_2, forming $BaTiO_3$ (Equation (3)). In particular, the solid-state synthesis reaction using two materials, $BaCO_3$ and TiO_2, involves the synthesis of $BaTiO_3$ through the unilateral diffusion of Ba^{2+} ions into TiO_2 [32].

In solid-state synthesis, the control of the surface characteristics, size, and morphology of TiO_2 is imperative for controlling the properties of $BaTiO_3$ [17]. The size effect has a significant impact on various properties of the powder [33,34]. In the case of TiO_2, for powder sizes of approximately 50 nm, the surface energy of rutile TiO_2 is high at 1.78–2.08 J/m^2, whereas that of anatase TiO_2 is considerably lower at 1.28–1.40 J/m^2. In particular, for small-size powders, rutile TiO_2 has a high surface energy, thereby showing superior reactivity at the surface and interface compared to that of anatase TiO_2 [35–37]. The application of heat treatment to TiO_2 powders results in the formation of powders with a composite phase comprising anatase and rutile phases, and TiO_2 powders with sizes of approximately 50 nm undergo phase transformation to the rutile phase (XRD, TEM). Specifically, the as-formed composite TiO_2 powders consist of larger-sized grains (~150 nm) in the anatase phase and smaller-sized grains (~50 nm) in the rutile phase. Among these TiO_2 powders, rutile TiO_2 powders with a grain size of 50 nm have a high surface energy, and after their surface contact with $BaCO_3$, the reaction rate could be faster than that of other large-sized powders during the formation of $BaTiO_3$. The rutile TiO_2 powders with smaller sizes react with $BaCO_3$ at the initial stages of the solid-state synthesis process. In contrast, anatase TiO_2 powders undergo the reaction with $BaCO_3$ at later stages of the synthesis process owing to their lower surface energy. During the solid-state reaction, the driving force for grain growth is determined by the mean grains size and grain size distribution. TiO_2 powders with smaller-sized grains react with $BaCO_3$ at the initial stages of synthesis, and grain growth progresses. Therefore, the average grain size of the synthesized $BaTiO_3$ could increase [38–42]. Such increases in the grain size are confirmed via the mean grain size analysis of $BaTiO_3$ synthesized at calcination temperatures of 1000 and 1100 °C using annealed TiO_2. A comparative analysis of the mean grain size of calcinated $BaTiO_3$ powders synthesized using composite TiO_2 and mixed TiO_2 was performed. The grain size of $BaTiO_3$ calcined at 1000 °C using composite

TiO_2 was approximately 250–280 nm. In addition, the grain size increased further to 270–445 nm at a calcination temperature of 1100 °C. However, when mixed TiO_2 was used for the solid-state synthesis, the $BaTiO_3$ grain size was smaller than that obtained using composite TiO_2 (Figure 8).

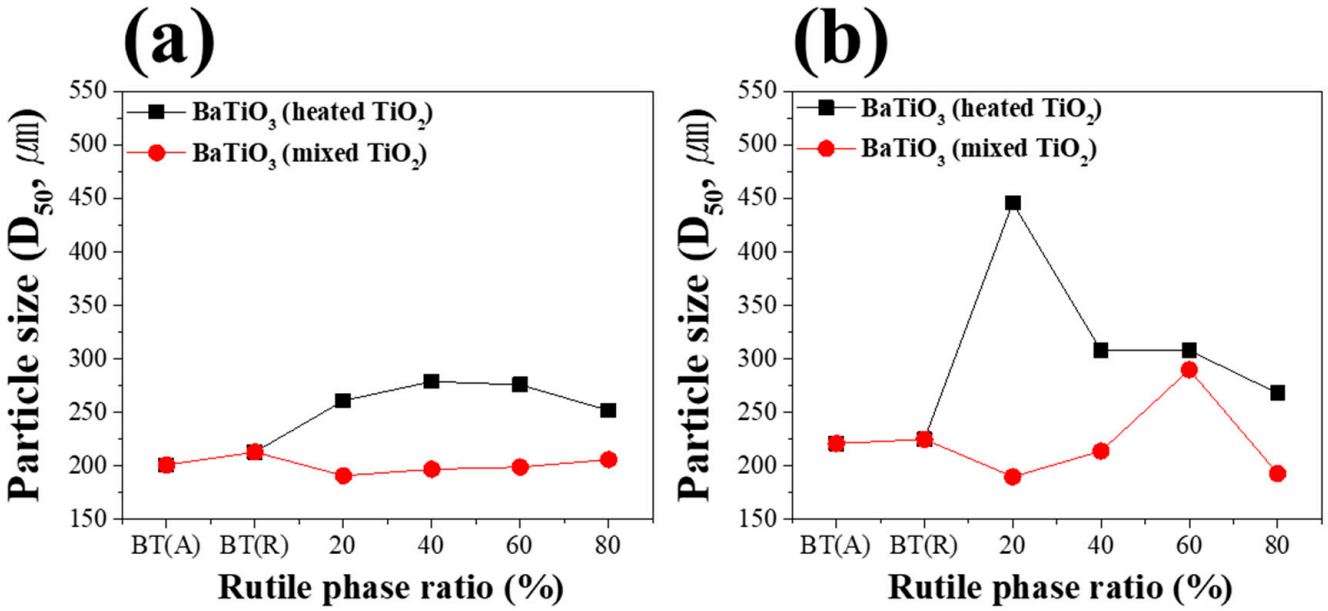

Figure 8. Comparative analysis of the mean particle size of $BaTiO_3$ powders obtained via solid-state synthesis at 1000 and 1100 °C using composite TiO_2 and mixed TiO_2. Solid-state synthesis conditions: (**a**) 1000 °C × 2 h and (**b**) 1100 °C × 2 h.

Powder compacts obtained under different conditions of BT(A) to BT#8 and calcinated at 1100 °C were sintered at 1300 °C for 2 h. Based on the microstructure analysis of the fractured surface of the specimens, grains with a size of 3 μm were observed in the sintered specimen prepared using the BT(A) powder. Furthermore, numerous pores were observed in the fractured surface analysis. In the case of the specimen prepared using the BT(R) powder, grains with a size of 2.3 μm were observed. For the specimens obtained using powders prepared under the synthesis conditions of BT#1 to BT#4, grains with sizes of 27.7–31.9 μm were observed. Although sintering densification did not occur under BT(A) and BT(R) conditions, under the conditions of BT#1 to BT#4 that used composite TiO_2, sufficient grain growth was observed. However, under the conditions of BT#5 to BT#8 that used a simple mixture of anatase and rutile TiO_2, sufficient grain growth, which was confirmed in the case of composite TiO_2, was not observed. A certain extent of grain growth was observed in the BT#8 powder, which had a relatively high fraction of the rutile phase (Figure 9).

The difference in the grain size of the sintered specimens according to the $BaTiO_3$ powder conditions can be explained using the step free energy related to the critical driving force for grain growth. When the shape of the grain is flat to show high anisotropy, the critical driving force for growth increases, and grain growth can be suppressed. However, when the grain surface is spherical, it forms an isotropic structure, and the step free energy decreases, resulting in a small critical driving force for grain growth. In particular, grain growth occurs more easily with a lower critical driving force. When the powders synthesized via the solid-state synthesis reaction using 100% anatase and 100% rutile TiO_2 are analyzed, flat-shaped grains with high anisotropy are observed (Figure 10). Moreover, in the case of the powders synthesized using the simple mixture of TiO_2, a similar flat and highly anisotropic morphology of the grains is observed. However, in the case of $BaTiO_3$ powders synthesized using the heated TiO_2 powder, the edges and vertices of the grains gradually change to form a spherical shape, creating an isotropic structure.

Therefore, $BaTiO_3$ powders using annealed TiO_2 are transformed to a state with a lower critical driving force for grain growth; therefore, grain growth can occur easily during sintering [42–44].

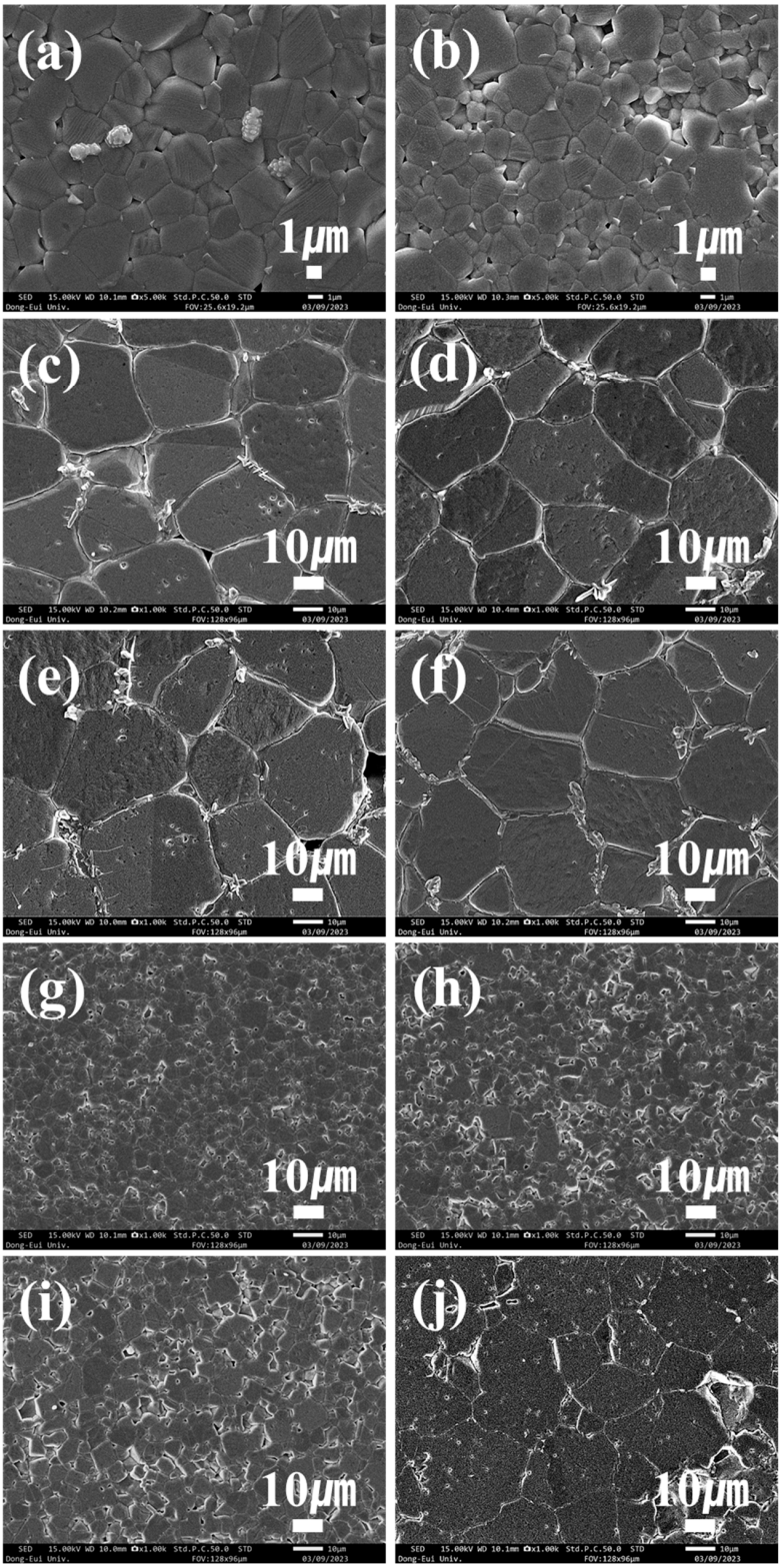

Figure 9. Fractured surface analysis of sintered specimens of $BaTiO_3$ powders obtained via solid-state synthesis under the conditions of 1000 °C × 2 h. Sintering conditions: 1300 °C × 2 h. (**a**) BT(A), (**b**) BT(R), (**c**) BT#1, (**d**) BT#2, (**e**) BT#3, (**f**) BT#4, (**g**) BT#5, (**h**) BT#6, (**i**) BT#7, and (**j**) BT#8.

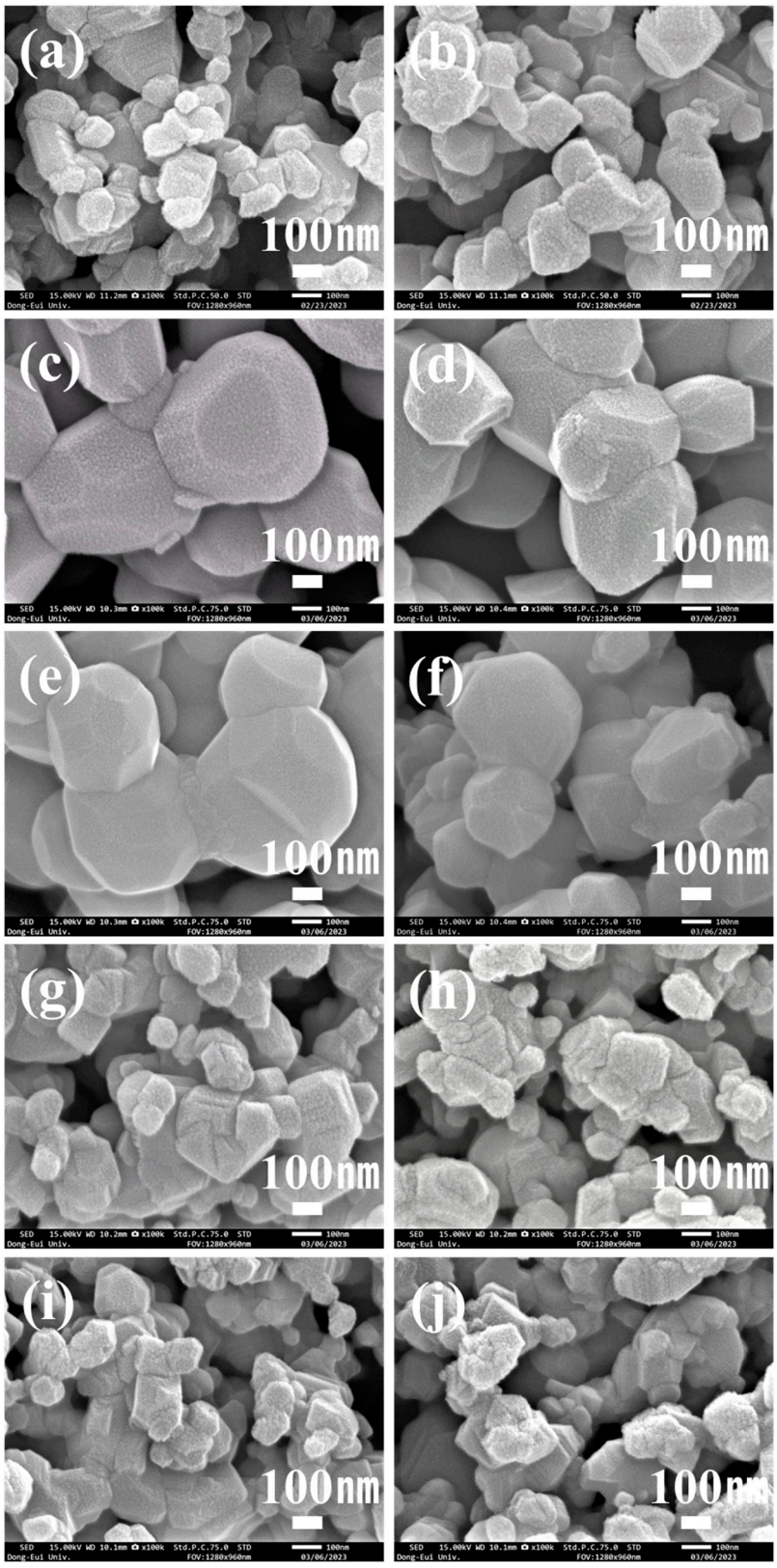

Figure 10. Microstructure analysis of solid-state-synthesized $BaTiO_3$ powders under the conditions of 1100 °C × 2 h (magnification: 100 k×). (**a**) BT(A), (**b**) BT(R), (**c**) BT#1, (**d**) BT#2, (**e**) BT#3, (**f**) BT#4, (**g**) BT#5, (**h**) BT#6, (**i**) BT#7, and (**j**) BT#8.

For powders synthesized via solid-state synthesis using composite TiO_2 under BT#1 to BT#4 conditions, a stable dielectric constant value of approximately 2400 was observed (Table 2). Moreover, when mixed TiO_2 was used for solid-state synthesis, the dielectric constant of the synthesized $BaTiO_3$ gradually decreased with an increasing rutile phase ratio (Figure 11). The dielectric constant is an essential piece of information when designing capacitors and in other circumstances where a material might be expected to introduce capacitance into a circuit. The dielectric constant is the ratio of the capacitance of the capacitor with test material as the dielectric to the capacitance of a capacitor with vacuum (or air) as the dielectric [45].

Table 2. Results of tetragonality and permittivity according to $BaTiO_3$ conditions (calcination condition: 1000 °C × 2 h, 1100 °C × 2 h).

$BaTiO_3$ Condition	1000 °C Calcination		1100 °C Calcination	
	Tetragonality (c/a)	Permittivity (ε_r)	Tetragonality (c/a)	Permittivity (ε_r)
BT#1	1.0094	2195	1.0102	2446
BT#2	1.0097	2162	1.0104	2357
BT#3	1.0094	2093	1.0104	2334
BT#4	1.0100	2129	1.0102	2408
BT#5	1.0048	3494	1.0087	3584
BT#6	1.0076	2380	1.0085	2561
BT#7	1.0060	1993	1.0083	1980
BT#8	1.0060	1891	1.0077	1721
BT(A)	1.0070	4042	1.0098	16,780
BT(R)	1.0065	1782	1.0094	1867

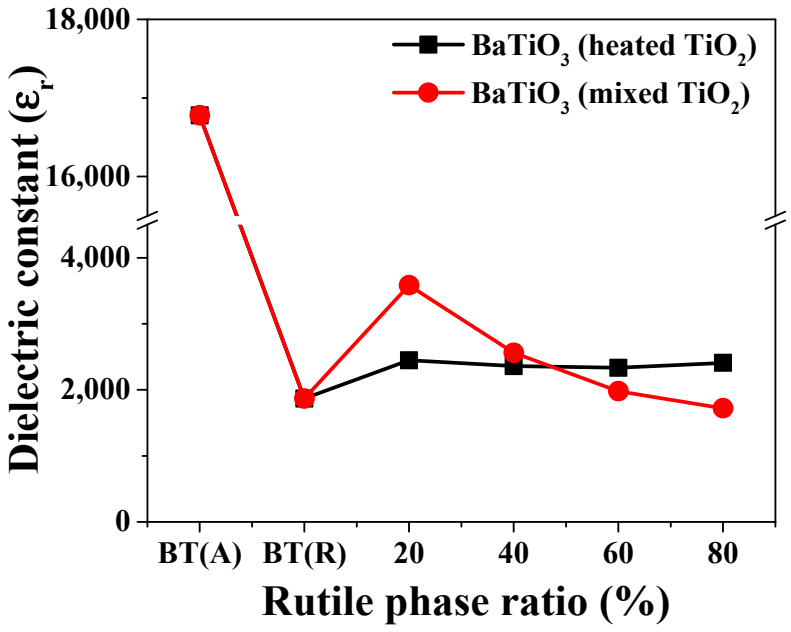

Figure 11. Evaluation of dielectric properties of sintered specimens obtained using solid-state-synthesized $BaTiO_3$ with composite TiO_2 and mixed TiO_2 (solid-state synthesis: 1100 °C × 2 h; sintering condition: 1300 °C × 2 h).

The changes in the dielectric constant were analyzed according to the temperature changes for the specimens sintered at 1300 °C with powders synthesized under the BT#1–BT#8 conditions, as shown in Figure 12. In the case of powders synthesized under the BT#1 to BT#4 conditions that used TiO_2 with a controlled anatase–rutile phase ratio through annealing, considerably high dielectric constant values were achieved near the Curie

temperature (T_c). However, for the powders prepared using simply mixed TiO_2, relatively low dielectric constant values were confirmed at T_c. $BaTiO_3$ exhibits a tetragonal crystal structure in the temperature range of ambient temperature–T_c, and when the temperature increases above T_c, the $BaTiO_3$ crystal structure changes to a cubic phase. Therefore, $BaTiO_3$ prepared using composite TiO_2 requires high activation energy for transformation from a tetragonal structure to a cubic structure, whereas in the case of $BaTiO_3$ formed using mixed TiO_2, the crystal structure can be changed with relatively low activation energy.

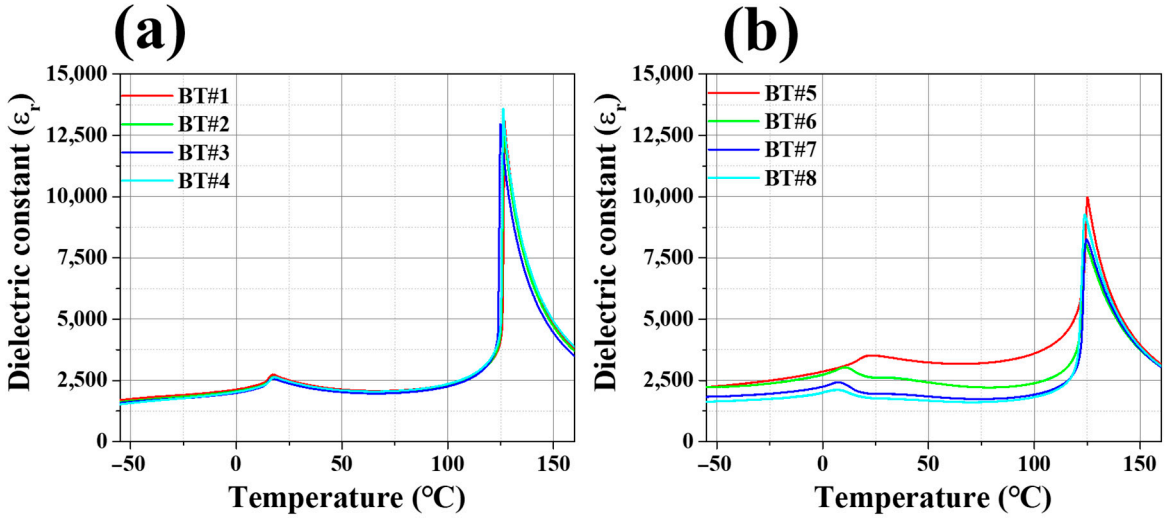

Figure 12. Dielectric constant as a function of temperature (Temperature range: −55–160 °C). Sintered specimens of solid-state-synthesized $BaTiO_3$ powder using (**a**) composite TiO_2 and (**b**) mixed TiO_2.

4. Conclusions

To improve the properties of ferroelectric $BaTiO_3$ powders used as raw materials for MLCCs, TiO_2 powders with different composite phase ratios were used for their synthesis, and a comparative analysis was performed in terms of the crystal structure, powder morphology, and dielectric properties. The main aspects of this study are as follows.

(1) Heat treatment was applied to anatase TiO_2 to achieve control of the composite phase structure with different anatase–rutile phase ratios.
(2) Using composite TiO_2 in the solid-state synthesis of $BaTiO_3$ is highly effective in improving tetragonality.
(3) Using composite TiO_2 in the solid-state synthesis of $BaTiO_3$ is effective in promoting grain growth of the powders. Furthermore, control of the powder morphology is achieved, and during sintering, the use of composite TiO_2 is advantageous for facilitating sintering densification at relatively low temperatures.
(4) $BaTiO_3$ synthesized using composite TiO_2 via the solid-state method exhibits a stable dielectric constant of approximately 2400 and effectively retains a tetragonal structure at ambient temperature.
(5) The use of composite TiO_2 is expected to be highly advantageous for fabricating MLCCs for use in the automotive and aerospace industries, where high-voltage applications with high reliability are of critical importance.

Author Contributions: Conceptualization, Y.K. and M.C. (Moonhee Choi); Methodology, S.-H.L. and Y.-S.L.; Software, K.-S.M.; Validation, S.-H.L. and Y.-S.L.; Formal analysis, J.K., J.-H.S. and R.-S.C.; Investigation, J.K., J.-H.S. and R.-S.C.; Resources, M.C. (Moonhee Choi); Data curation, M.C. (Myunghee Cho) and H.K.; Writing—original draft, S.-H.L.; Writing—review & editing, Y.-S.L., Y.K., K.-S.M. and M.C. (Moonhee Choi); Visualization, S.C.; Supervision, Y.K., K.-S.M. and M.C. (Moonhee Choi); Project administration, M.C. (Moonhee Choi); Funding acquisition, M.C. (Moonhee Choi). All authors have read and agreed to the published version of the manuscript.

Funding: This study was supported by the Materials and Parts Technology Development Program (Grant No. 20010938), funded by the Ministry of Trade, Industry and Energy (MoTIE, Republic of Korea). This work was supported by the Institute for Information and Communications Technology Promotion (IITP) grant funded by the Korea Government (MSIP) (No. 2021-0-00793).

Institutional Review Board Statement: Not applicable.

Informed Consent Statement: Not applicable.

Data Availability Statement: Not applicable.

Conflicts of Interest: The authors declare that they have no known competing financial interests or personal relationships that could have appeared to influence the work reported in this paper.

References

1. Zhu, C.; Zhao, Q.; Cai, Z.; Guo, L.; Li, L.; Wang, X. High reliable non-reducible ultra-fine $BaTiO_3$-based ceramics fabricated via solid-state method. *J. Alloys Compd.* **2020**, *829*, 154496. [CrossRef]
2. Zhu, C.; Cai, Z.; Cao, X.; Fu, Z.; Li, L.; Wang, X. High-dielectric-constant nanograin $BaTiO_3$-based ceramics for ultra-thin layer multilayer ceramic capacitors via grain grading engineering. *Adv. Powder Mater.* **2022**, *1*, 100029. [CrossRef]
3. Pan, M.-J.; Randall, C.A. A brief introduction to ceramic capacitors. *IEEE Electr. Insul. Mag.* **2010**, *26*, 44–50. [CrossRef]
4. Hong, K.; Lee, T.H.; Suh, J.M.; Yoon, S.-H.; Jang, H.W. Perspectives and challenges in multilayer ceramic capacitors for next generation electronics. *J. Mater. Chem. C* **2019**, *7*, 9782–9802. [CrossRef]
5. Hennings, D.; Schreinemacher, S. Characterization of hydrothermal barium titanate. *J. Eur. Ceram. Soc.* **1992**, *9*, 41–46. [CrossRef]
6. Wada, S.; Suzuki, T.; Noma, T. Preparation of barium titanate fine particles by hydrothermal method and their characterization. *J. Ceram. Soc. Jpn.* **1995**, *103*, 1220–1227. [CrossRef]
7. Li, J.; Inukai, K.; Tsuruta, A.; Takahashi, Y.; Shin, W. Synthesis of highly disperse tetragonal $BaTiO_3$ nanoparticles with core–shell by a hydrothermal method. *J. Asian Ceram. Soc.* **2017**, *5*, 444–451. [CrossRef]
8. Lencka, M.M.; Riman, R.E. Thermodynamic modeling of hydrothermal synthesis of ceramic powders. *Chem. Mater.* **1993**, *5*, 61–70. [CrossRef]
9. Chen, H.-J.; Chen, Y.-W. Hydrothermal synthesis of barium titanate. *Ind. Eng. Chem. Res.* **2003**, *42*, 473–483. [CrossRef]
10. Hennings, D.F.; Metzmacher, C.; Schreinemacher, B.S. Defect chemistry and microstructure of hydrothermal barium titanate. *J. Am. Ceram. Soc.* **2001**, *84*, 179–182. [CrossRef]
11. Baek, C.; Wang, J.E.; Moon, S.; Choi, C.H.; Kim, D.K. Formation and accumulation of intragranular pores in the hydrothermally synthesized barium titanate nanoparticles. *J. Am. Ceram. Soc.* **2016**, *99*, 3802–3808. [CrossRef]
12. Vengrenovitch, R. On the Ostwald ripening theory. *Acta Metall.* **1982**, *30*, 1079–1086. [CrossRef]
13. Choi, S.H.; Lee, Y.-S.; Lee, S.H.; Beak, K.; Cho, S.; Jo, I.; Kim, Y.; Moon, K.-S.; Choi, M. Enhancement of dielectric properties and microstructure control of $BaTiO_3$ by seed-induced solid-state synthesis. *Ceram. Int.* **2023**, *49*, 17921–17929. [CrossRef]
14. Lim, J.-C.; Kim, S.-I.; Hong, G.-H.; Hwang, J.-H.; Yang, H.; Lee, K.H.; Kim, H.-S. Skewness: Important parameter to affect the dielectric properties of $BaTiO_3$. *J. Asian Ceram. Soc.* **2022**, *10*, 613–620. [CrossRef]
15. Othman, K.I.; Hassan, A.A.; Abdelal, O.A.; Elshazly, E.S.; Ali, M.E.-S.; El-Raghy, S.; El-Houte, S. Formation mechanism of barium titanate by solid-state reactions. *Int. J. Sci. Eng. Res.* **2014**, *5*, 1460–1465.
16. Awan, I.T.; Pinto, A.H.; Nogueira, I.; Bezzon, V.; Leite, E.; Balogh, D.T.; Mastelaro, V.R.; Ferreira, S.E.M., Jr. Insights on the mechanism of solid state reaction between TiO_2 and $BaCO_3$ to produce $BaTiO_3$ powders: The role of calcination, milling, and mixing solvent. *Ceram. Int.* **2020**, *46*, 2987–3001. [CrossRef]
17. Pithan, C.; Hennings, D.; Waser, R. Progress in the synthesis of nanocrystalline $BaTiO_3$ powders for MLCC. *Int. J. Appl. Ceram. Technol.* **2005**, *2*, 1–14. [CrossRef]
18. Buscaglia, M.T.; Bassoli, M.; Buscaglia, V.; Vormberg, R. Solid-state synthesis of nanocrystalline $BaTiO_3$: Reaction kinetics and powder properties. *J. Am. Ceram. Soc.* **2008**, *91*, 2862–2869. [CrossRef]
19. Lee, T.; Jung, H.; Song, Y.; Cho, S.; Kim, D.-H.; Kim, Y.; Lee, Y.-S.; Park, Y.; Choi, M. Development of a Highly Densified Magnetic Sheet for Inductors and Advanced Processes through Silane Surface Treatment of Fe Nanopowder. *Appl. Sci.* **2020**, *10*, 4770. [CrossRef]
20. Choi, S.H.; Lee, Y.-S.; Kwak, H.; Jung, H.J.; Kim, M.; Cho, S.; Yoon, J.H.; Choi, J.W.; Kim, M.S.; Kim, J.H. Major factors affecting the dielectric properties and reliability of solid stated reacted $BaTiO_3$ powders for capacitor. *J. Asian Ceram. Soc.* **2022**, *10*, 713–721. [CrossRef]
21. Beak, K.; Choi, M.; Kim, D.H.; Yu, Y.; Theerthagiri, J.; Al-Mohaimeed, A.M.; Kim, Y.; Jung, H.J.; Choi, M.Y. Silane-treated $BaTiO_3$ ceramic powders for multilayer ceramic capacitor with enhanced dielectric properties. *Chemosphere* **2022**, *286*, 131734. [CrossRef] [PubMed]
22. Arbiol, J.; Cerda, J.; Dezanneau, G.; Cirera, A.; Peiro, F.; Cornet, A.; Morante, J. Effects of Nb doping on the TiO_2 anatase-to-rutile phase transition. *J. Appl. Phys.* **2002**, *92*, 853–861. [CrossRef]
23. Hu, Y.; Tsai, H.-L.; Huang, C.-L. Phase transformation of precipitated TiO_2 nanoparticles. *Mater. Sci. Eng. A* **2003**, *344*, 209–214. [CrossRef]

24. Hanaor, D.A.; Sorrell, C.C. Review of the anatase to rutile phase transformation. *J. Mater. Sci.* **2011**, *46*, 855–874. [CrossRef]
25. Myint, Y.W.; Moe, T.T.; Linn, W.Y.; Chang, A.; Win, P.P. The effect of heat treatment on phase transformation and morphology of nano-crystalline titanium dioxide (TiO_2). *Int. J. Sci. Technol. Res.* **2017**, *6*, 293–299. [CrossRef]
26. Zhu, X.; Han, S.; Feng, W.; Kong, Q.; Dong, Z.; Wang, C.; Lei, J.; Yi, Q. The effect of heat treatment on the anatase–rutile phase transformation and photocatalytic activity of Sn-doped TiO_2 nanomaterials. *RSC Adv.* **2018**, *8*, 14249–14257. [CrossRef]
27. Perego, C.; Revel, R.; Durupthy, O.; Cassaignon, S.; Jolivet, J.-P. Thermal stability of TiO_2-anatase: Impact of nanoparticles morphology on kinetic phase transformation. *Solid State Sci.* **2010**, *12*, 989–995. [CrossRef]
28. Kumar, L.; Kumar, P.; Narayan, A.; Kar, M. Rietveld analysis of XRD patterns of different sizes of nanocrystalline cobalt ferrite. *Int. Nano Lett.* **2013**, *3*, 1–12. [CrossRef]
29. Zali, N.M.; Mahmood, C.S.; Mohamad, S.M.; Foo, C.T.; Murshidi, J.A. X-ray diffraction study of crystalline barium titanate ceramics. In *AIP Conference Proceedings*; American Institute of Physics: College Park, MD, USA, 2014; pp. 160–163. [CrossRef]
30. Sakabe, Y. Grain Size Effects on Dielectric Properties and Crystal Structure of Fine-Grained $BaTiO_3$ Ceramics. *J. Korean Phy. Soc.* **1998**, *32*, 260–264.
31. Yoon, D. Tetragonality of barium titanate powder for a ceramic capacitor application. *J. Ceram. Process. Res.* **2006**, *7*, 343.
32. Beauger, A.; Mutin, J.; Niepce, J. Synthesis reaction of metatitanate $BaTiO_3$: Part 2 Study of solid-solid reaction interfaces. *J. Mater. Sci.* **1983**, *18*, 3543–3550. [CrossRef]
33. Almquist, C.B.; Biswas, P. Role of synthesis method and particle size of nanostructured TiO_2 on its photoactivity. *J. Catal.* **2002**, *212*, 145–156. [CrossRef]
34. Hoshina, T. Size effect of barium titanate: Fine particles and ceramics. *J. Ceram. Soc. Jpn.* **2013**, *121*, 156–161. [CrossRef]
35. Zhang, H.; Banfield, J.F. Structural characteristics and mechanical and thermodynamic properties of nanocrystalline TiO_2. *Chem. Rev.* **2014**, *114*, 9613–9644. [CrossRef]
36. Chen, Y.; Wang, Y.; Li, W.; Yang, Q.; Hou, Q.; Wei, L.; Liu, L.; Huang, F.; Ju, M. Enhancement of photocatalytic performance with the use of noble-metal-decorated TiO_2 nanocrystals as highly active catalysts for aerobic oxidation under visible-light irradiation. *Appl. Catal. B Environ.* **2017**, *210*, 352–367. [CrossRef]
37. Jovic, V.; Al-Azri, Z.H.; Chen, W.-T.; Sun-Waterhouse, D.; Idriss, H.; Waterhouse, G.I. Photocatalytic H_2 production from ethanol–water mixtures over Pt/TiO_2 and Au/TiO_2 photocatalysts: A comparative study. *Top. Catal.* **2013**, *56*, 1139–1151. [CrossRef]
38. Suk-Joong, L.; Han, S.-M. Grain Growth in Si_3N_4-Based Materials. *MRS Bull.* **1995**, *20*, 33–37. [CrossRef]
39. Park, Y.J.; Hwang, N.M.; Yoon, D.Y. Abnormal growth of faceted (WC) grains in a (Co) liquid matrix. *Metall. Mater. Trans. A* **1996**, *27*, 2809–2819. [CrossRef]
40. Yoon, D.Y. The Step Growth Hypothesis for Abnormal Grain Growth. International Workshop on Ceramic Interfaces. 2001, pp. 3–21. Available online: http://hdl.handle.net/10203/135758 (accessed on 1 December 2018).
41. Kim, M.S.; Fisher, J.G.; Kang, S.J.L.; Lee, H.Y. Grain growth control and solid-state crystal growth by Li_2O/PbO addition and dislocation introduction in the PMN–35PT system. *J. Am. Ceram. Soc.* **2006**, *89*, 1237–1243. [CrossRef]
42. Moon, K.S.; Kang, S.J.L. Coarsening behavior of round-edged cubic grains in the $Na_{1/2}Bi_{1/2}TiO_3$–$BaTiO_3$ system. *J. Am. Ceram. Soc.* **2008**, *91*, 3191–3196. [CrossRef]
43. Kang, S.-J.L. *Sintering: Densification, Grain Growth and Microstructure*; Elsevier Butterworth-Heinemann: Oxford, UK, 2005. [CrossRef]
44. Moon, K.-S.; Rout, D.; Lee, H.-Y.; Kang, S.-J.L. Effect of TiO_2 addition on grain shape and grain coarsening behavior in $95Na_{1/2}Bi_{1/2}TiO_3$–$5BaTiO_3$. *J. Eur. Ceram. Soc.* **2011**, *31*, 1915–1920. [CrossRef]
45. McKeen, L.W. *Film Properties of Plastics and Elastomers*; William Andrew: Norwich, NY, USA, 2017. [CrossRef]

Disclaimer/Publisher's Note: The statements, opinions and data contained in all publications are solely those of the individual author(s) and contributor(s) and not of MDPI and/or the editor(s). MDPI and/or the editor(s) disclaim responsibility for any injury to people or property resulting from any ideas, methods, instructions or products referred to in the content.